Ecotoxicology and Environmental Safety 260 (2023) 115019

Contents lists available at ScienceDirect

Ecotoxicology and Environmental Safety

journal homepage: www.elsevier.com/locate/ecoenv

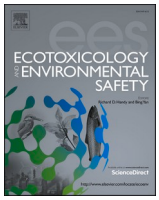

The influence of size and surface chemistry on the bioavailability, tissue distribution and toxicity of gold nanoparticles in zebrafish (*Danio rerio*)

Dylan L. Windell [a], Sulayman Mourabit [a], Julian Moger [b], Stewart F. Owen [c], Matthew J. Winter [a], Charles R. Tyler [a,*]

[a] Biosciences, Faculty of Health and Life Sciences, Exeter, Devon EX4 4QD, United Kingdom
[b] Physics and Medical Imaging, College of Engineering, Mathematics and Physical Sciences, University of Exeter, Exeter, Devon EX4 4QL, United Kingdom
[c] AstraZeneca, Global Compliance, Alderley Park, Macclesfield, Cheshire SK10 4TF, United Kingdom

ARTICLE INFO

Edited by Professor Bing Yan

Keywords:
SPIM
Light sheet microscopy
Gold nanoparticles
Nanotoxicology
Zebrafish

ABSTRACT

Gold nanoparticles (AuNPs) are widely used in biomedicine and their specific properties including, size, geometrics, and surface coating, will affect their fate and behaviour in biological systems. These properties are well studied for their intended biological targets, but there is a lack of understanding on the mechanisms by which AuNPs interact in non-target organisms when they enter the environment. We investigated the effects of size and surface chemistry of AuNPs on their bioavailability, tissue distribution and potential toxicity using zebrafish (*Danio rerio*) as an experimental model. Larval zebrafish were exposed to fluorescently tagged AuNPs of different sizes (10–100 nm) and surface modifications (TNFα, NHS/PAMAM and PEG), and uptake, tissue distribution and depuration rates were measured using selective-plane illumination microscopy (SPIM). The gut and pronephric tubules were found to contain detectable levels of AuNPs, and the concentration-dependent accumulation was related to the particle size. Surface addition of PEG and TNFα appeared to enhance particle accumulation in the pronephric tubules compared to uncoated particles. Depuration studies showed a gradual removal of particles from the gut and pronephric tubules, although fluorescence indicating the presence of the AuNPs remained in the pronephros 96 h after exposure. Toxicity assessment using two transgenic zebrafish reporter lines, however, revealed no AuNP-related renal injury or cellular oxidative stress. Collectively, our data show that AuNPs used in medical applications across the size range 40–80 nm, are bioavailable to larval zebrafish and some may persist in renal tissue, although their presence did not result in measurable toxicity with respect to pronephric organ function or cellular oxidative stress for short term exposures.

1. Introduction

The use of nanoparticles for biomedical applications including imaging, drug delivery and directly as medicines has increased dramatically in recent years. Crucially, nanomedicines can cross a wide range of biological membranes (including the blood-brain barrier), aiding the diagnosis and treatment of a range of life-threatening diseases. AuNPs are particularly well suited as drug carriers due to their inert properties, and ability to be coated with biocompatible materials, which can be functionalised with proteins to facilitate uptake into specific tissues (Khan et al., 2014; Nicol et al., 2015; Daraee et al., 2016). Thus, AuNP design can be tailored for specific applications in a process that often includes attachment of several biocompatible materials onto a AuNP (Nicol et al., 2015). Specific examples of AuNP modifications include: coatings or stabilising agents such as polylactic acid (PLA) (Qiu et al., 2004); polyethylene glycol (PEG) (Aryal et al., 2009; Choi et al., 2010); bovine serum albumin (BSA) (Leopold et al., 2017); amine groups (Lee et al., 2008); or attachment of materials such as chitosan (Boyles et al., 2015), peptides (Satriano et al., 2018), oligosaccharides (Manivasagan et al., 2016) or antibodies (García-Fernández et al., 2017). Other modifications include AuNPs shape and manipulation of their surface charge in order to promote increased biocompatibility (Verma et al., 2018).

With an increased focus on novel drug delivery technologies, it is likely that more AuNP-based therapeutics will be developed and inevitably this will lead to greater release into the aquatic environment. Evaluations of the potential impacts of AuNPs in the aquatic environment are therefore greatly needed (Corsi et al., 2014; Khosravi-Katuli et al., 2017). Previous studies have investigated the impact of altered

* Correspondence to: Biosciences, Faculty of Health and Life Sciences, University of Exeter, Geoffrey Pope Building, Exeter, Devon EX4 4QD, United Kingdom.
E-mail address: C.R.Tyler@exeter.ac.uk (C.R. Tyler).

https://doi.org/10.1016/j.ecoenv.2023.115019
Received 31 January 2023; Received in revised form 5 May 2023; Accepted 14 May 2023
Available online 1 June 2023

AuNP physiochemistry on particle uptake into mammalian cell lines (Chithrani et al., 2006; Oh et al., 2011), and shown the importance of composition including particle size, shape, structure, chemical composition and functionalisation (Fratoddi et al., 2015; Carnovale et al., 2016; Libralato et al., 2017). Far less is known, however, about the effects of nanodrug carrier systems in vivo, or in aquatic organisms specifically. Recent studies have started to investigate the potential toxic effects of various AuNP sizes, shapes, coatings and attachments in aquatic organisms (Bozich et al., 2014; Botha et al., 2015; Dominguez et al., 2015; Park et al., 2015; Wang et al., 2016; Sung et al., 2018; Van Pomeren et al., 2019), however, they have focused on very specific (and often different) NP characteristics, making comparisons between frequently conflicting findings difficult.

To address this knowledge gap, we investigated both the influence of AuNP size and differences in surface chemistry on particle bioavailability, tissue distribution, elimination, and toxicity in zebrafish (*Danio rerio*) using multiple imaging modalities. Firstly, we exposed zebrafish (up to 7 days post-fertilisation or dpf) to 5 fluorescently tagged AuNPs of different sizes (10–100 nm in diameter) in aqueous suspensions, and quantified subsequent particle uptake, tissue distribution and clearance. Next, we assessed the impact of three surface modifications used widely in biomedical applications (tumour necrosis factor α (TNFα), N-hydroxysuccinimide/polyamidoamine (NHS/PAMAM) and PEG) on the same parameters using 80 nm AuNPs. Finally, after identifying the larval zebrafish pronephros as a potential target for AuNP toxicity, we used a zebrafish transgenic fluorescent reporter line (Zhou and Hildebrandt, 2012) to assess the potential impact of AuNP on pronephric function. We also applied a second zebrafish reporter line to assess AuNP-induced cellular oxidative stress as this is an identified toxicity pathway associated with nanoparticle exposure in animal studies, including zebrafish (Geffroy et al., 2012; Dedeh et al., 2015; Mourabit et al., 2019).

2. Materials and methods

2.1. AuNP preparation

DiagNano™ gold nanoparticles (spherical colloidal gold) used in this study had a functional non-reactive Methyl Polymer layer and an Alexa Fluor 488 nm fluorophore layer (Creative Diagnostics, New York, USA). This non-toxic multi-layered heterogeneous polymer comprising of a mixed brush polymer (with 500 Da segments and 2.5 kDa segments) which reduces/eliminates ionic or non-specific binding. The Alexa Fluor 488 nm fluorophore layer facilitates fluorescence microscopic visualisation for accurate particle localisation in vivo. The standard AuNP sizes used were 10, 20, 40, 80 and 100 nm in diameter with the original stock manufactured and stored in 1 × E3 Medium. The zebrafish E3 medium (pH 7.0 (± 0.05) consisted of 5.0 mM NaCl (292 mg/L), 0.17 mM KCl (13 mg/L), 0.33 mM CaCl (44 mg/L) and 0.33 mM MgSO4 (81 mg/L) dissolved in MilliQ water.

For investigations into the effects of surface modifications, the standard 80 nm DiagNano™ AuNPs were subject to three modifications: 1) addition of TNFα to the outer surface. 2) addition of an NHS group allowing for the subsequent additional conjugation of PAMAM dendrimers (Generation 0.0, Sigma-Aldrich, UK) and, 3) substituting the polymer coating with PEG.

The PEG and TNFα AuNPs were supplied in conjugated forms in 1x E3 medium. The NHS AuNP was provided as a solid powder as NHS is not stable in aqueous solution and readily undergoes hydrolysis. NHS AuNP was therefore first modified with the addition of PAMAM dendrimers (w/ethylenediamine cores in a methanol solution) to stabilise the NHS groups. For this, 1 ml of PAMAM dendrimer solution (500-fold) was added to 2.5 mg of 80 nm NHS AuNP in a plastic eppendorf, the suspension sonicated for 1 min (35 kHz), and vortexed for 30 min at 28 °C to facilitate PAMAM binding. During the period of vortexing, the resultant suspension was sonicated every 10 min to ensure the AuNPs were fully suspended. This suspension was then purified by centrifuging at 9700 g, removing the supernatant (methanol) and re-suspending the pellet in fresh 1 × E3 medium. This purification process was repeated three times and finally the AuNPs were resuspended in 1 × E3 medium and stored at 2–4 °C until required (this form is stable for up to 6 months).

2.2. Confirmation of AuNP characteristics

To confirm AuNP particle size and shape, TEM analysis was performed on the raw 10, 20, 40, 80 and 100 nm AuNPs, and on the modified 80 nm AuNPs. For this, 50 individual particles were measured for each size group (see Supplementary Figs. 1 and 2). Negative staining of the AuNPs involved placing a droplet of 2 mg/L AuNP suspensions on piloform-coated EM 100 mesh grids. These were then washed 4 times in deionised water (5 s each) and the preparation left to air dry before analysis using a JEOL JEM 1400 TEM operated at 120 kV and a digital camera (ES 100 W CCD, Gatan, Abingdon, UK). A second batch of unmodified 80 nm AuNPs was used to produce the surface coated particles. These had an equivalent concentration (5 mg/L), fluorescent level (± 10 % balance) and optical density (50) to the modified AuNPs (TNFα, PEG and NHS). For additional information on the particle characteristics see Supplementary Table 1.

Particle size and zeta potential measurements were performed with a Malvern Zetasizer (Malvern Instruments, University of Birmingham). The absorption was measured using a Jenway 6800 UV/Vis Spectrophotometer with a refractive index of 1.4 (Chen et al., 2008; Nejdl et al., 2016) and absorption of 1. The medium in which the AuNPs were stored (1 × E3 medium) acted as the baseline (blank). The temperature was set at 25 °C and the viscosity to that of 0.8872 centipoise (cP). The measurements were performed in disposable cuvettes (ZEN0040, Malvern Panalytical) containing 1 ml of AuNP suspension that were vortexed prior to taking measurements. The equilibration ran for 2 min with a measurement angle of 173° backscatter. Calculations were based on the Smoluchowski model with aF(κa) of 1.50. All measurements were performed in quadruplets using automatic attenuation and voltage selection and data expressed as the mean ± SD (See Table 2 for results).

2.3. Zebrafish models and husbandry

Three different zebrafish lines were used in this study. These included a *Casper* double mutant (nacrew2/w2;roya9/a9 (White et al., 2008)), a zebrafish that lacks skin pigmentation that was used to visualise AuNP uptake and depuration. The second line was pod::*NTR-mCherry/L-fabp::VDBP-GFP*, a double transgenic fluorescent reporter model (Kindly supplied by Dr. Weibin Zhou, University of Michigan, Ann Arbor) that was used for assessing pronephric renal injury. In this line, hepatic synthesis of VDBP-GFP (Vitamin D-binding protein-GFP fusion protein) is driven by the L-fabp promotor to provide a size and charge-selected tracer to indicate glomerular filtration barrier and subsequent proteinuria (Zhou and Hildebrandt, 2012). This model also has mCherry-labelled podocytes which form the glomerular filtration barrier (GFB), thus facilitating visual assessment of pronephric tubule morphology and GFB integrity. We first crossed this line into a *Casper* background to facilitate visualisation of the kidney tubule and any accumulating AuNPs. The third zebrafish line used in this work was a *3EpRE:hsp70:mCherry* transgenic fluorescent reporter line (Mourabit et al., 2019) that enabled us to visualise cellular level, tissue specific reactive oxygen species (ROS) production and oxidative stress in response to AuNP exposure.

2.4. Exposure of zebrafish embryo-larvae to nanoparticles

Immediately prior to each zebrafish exposure, a fresh suspension of gold particles was made from dilution of the stock solution (prepared in 1 × E3 medium, see below). The stock solution was vortexed for 5 min and sonicated (35 kHz) for an additional 5 min before making the

diluted suspensions for the exposures (Transonic T310, Camlab limited, Cambridge, UK). Once diluted in fresh 1x E3 medium, the suspension underwent mixing (vortexing and sonication, 5 min each), and the sonicated suspension was then used immediately for the zebrafish exposures. For all exposures, individual embryo-larvae were placed in a 24 well microtiter plates each with 1 ml suspensions of AuNPs (or 1 × E3 medium for controls) at 28 °C ± 1 °C on a plate mixer to prevent/reduce AuNP precipitation and aggregation for the duration of the exposure. Exposure media was not changed for the assessment of multi-sized or modified AuNP experiments. Media was changed for the depuration study but not with the addition of AuNP exposure media which was not added in any of the experiments performed.

A summary overview of all zebrafish exposure experiments detailed in the following sections is shown in Fig. 1.

2.5. Assessment of AuNP accumulation, distribution and elimination

Manually dechorionated *Casper* embryo-larvae were exposed to AuNPs (at size diameters of 10, 20, 40, 80 and 100 nm) for 72 h, from 1 dpf to 4 dpf when they were imaged using SPIM. For each exposure, three independent experiments were carried out with 6 fish for each AuNP concentration, alongside untreated controls (n = 18). The concentrations used for all particle sizes tested were 0.25, 0.5, 1 and 2 mg/L. For the 2 mg/L suspensions the molar concentrations for the different sized AuNP were 0.34 nM (10 nm), 0.026 pM (20 nm), 0.056 nM, (40 nm), 0.71 pM (80 nm) and 0.37 pM (100 nm) with the number of particles calculated at 2.14×10^{11} (10 nm), 2.73×10^{10} (20 nm), 3.48×10^{9} (40 nm), 4.43×10^{8} (80 nm) and 2.28×10^{8} (100 nm), respectively.

To assess clearance of uptaken AuNPs, *Casper* embryo-larvae were exposed to 40 nm and 80 nm AuNPs, and surface modified forms of these AuNPs from 2 to 3 dpf, and assessments were made after two periods (24 and 72 h) of depuration. 40 nm and 80 nm sized AuNPs were chosen for these studies as they were shown to accumulate in tissues in the first series of exposures. Exposure concentrations for the 40 nm and 80 nm sized AuNPs were 0.25, 0.5, 1 and 2 mg/L and for the NHS and Standard (control) AuNPs, the two higher doses only (1 and 2 mg/L) due to very low uptake rates at the lower concentrations. Following the AuNP exposures, animals were transferred to E3 medium without AuNPs for assessing clearance over time (each embryo-larvae was imaged at 3, 4 and 7 dpf) using SPIM. Prior to imaging, animals were transferred to fresh E3 medium in a new microtiter plate. Two independent experiments were conducted with 8 embryo-larvae for each AuNP concentration and untreated controls (n = 16 for each treatment).

After the exposures, animals were transferred into an Eppendorf containing 1x E3 medium to rinse off any externally adhered nanoparticles. Each individual embryo-larvae were then anaesthetised in 0.4 g/L tricaine methanesulfonate (pH 7, MS222, Sigma-Aldrich, UK) until immobile, or at 2 g/L to euthanise embryo-larvae older than 4 dpf. Anaesthetised embryo-larvae were then placed into 0.7 % low melting agarose containing MS222 at the above concentration to avoid residual movement during image acquisition. For SPIM analysis, using a 1 ml syringe, the embryo-larvae were drawn into a borosilicate capillary tube (940 μM internal diameter), tail first, which was then plugged with 1.5 % low melting point agarose. The mounted embryo-larvae were then placed head down in the sample chamber and the chamber was filled with 1 × E3 medium to allow the water-dipping lenses to focus appropriately.

For SPIM analysis of AuNP uptake, tissue distribution and elimination, we used an OpenSPIM system (see Supplementary Fig. 3), as described previously (Winter et al., 2017) with acquisition settings aimed at maximising image resolution. Full details on the operation and settings used for the OpenSPIM work are described in the Supplementary information (including Supplementary Fig. 4). The SPIM system allowed for a rapid and relatively high through-put capability for assessing the uptake of the AuNPs.

In addition to SPIM, a Leica TCS SP5 (Leica Microsystems, Milton Keynes, UK) laser scanning confocal microscope was used to acquire high resolution Z-stacks of the AuNP to illustrate their accumulation in the pronephric tubules of *Casper* embryo-larvae. This approach with

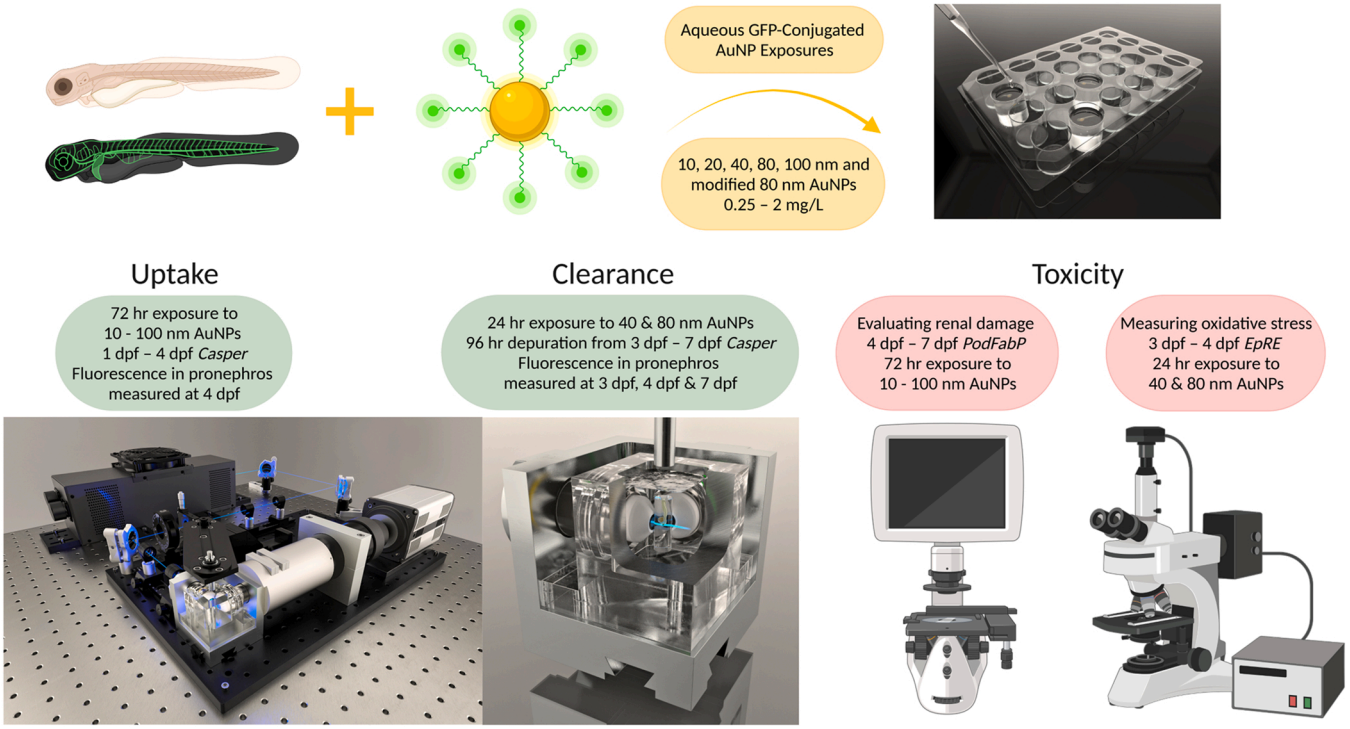

Fig. 1. Diagrammatic representation of the studies conducted, experimental model used and endpoints measured. Experiments conducted; Uptake of AuNPs into 4 dpf *Casper* zebrafish embryo-larvae, Clearance of AuNP uptaken in 7 dpf *Casper* embryo-larvae and measurement of toxicity caused by exposure to AuNPs in zebrafish embryo-larvae using a *PodFabP* transgenic to evaluate renal damage and an electrophile response element (*EpRE*) transgenic to measure oxidative stress.

high-resolution co-focal imaging allowed us to gain a clearer view on the AuNP distribution with the target tissues. Here, the following settings were applied: 1024 × 1024 12-bit images, 100 Hz line acquisition rate using an average of 4, smart gain of 900 with a − 1.2 offset and a pinhole size of 85 μm with 3 × artificial zoom. The Alexa 488 laser and GFP filterset were used with 25 % Argon laser power.

2.6. Assessment of pronephric renal injury

Our observation of accumulation of 40 nm and 80 nm AuNPs in the pronephric tubule, directed us to assess their effects on kidney morphology and function. This was undertaken in 7 dpf *pod*::NTR-mCherry/*L-fabp*::VDBP-GFP zebrafish. Animals of this age were used as clearer images of the developing pronephric tubule and more intense VDBP-GFP fluorescence occurred compared with 4 dpf embryo-larvae (*unpublished observations*). 4 dpf embryo-larvae were exposed for 72 h and imaged at 7 dpf using a wide-field fluorescence microscope (EVOS, Thermo Fisher Scientific, Waltham, MA). To assess the effect of AuNP concentration, two independent experiments were conducted with 40 and 80 nm AuNPs, with 8 zebrafish embryo-larvae used for each AuNP concentration (0.25–2 mg/L) alongside untreated controls (n = 16). To further assess the impact of size, an additional single exposure study was carried out using 10, 20 and 100 nm AuNPs at an exposure concentration of 2 mg/ml (n = 8 for each treatment).

After exposure, animals were transferred into an Eppendorf containing 1 × E3 medium to rinse off any externally adhered nanoparticles. Each individual embryo-larvae were then anaesthetised (as described above) and placed into 0.7 % agarose containing MS222 at the same concentration. Embryo-larvae were then mounted on their side on a glass microscope slide in 0.7 % agarose containing 0.4 g/L MS222. mCherry and GFP fluorescence was assessed using a wide-field fluorescence imaging system (EVOS, Thermo Fisher Scientific, Waltham, MA). The image settings used were as follows: 25 % brightfield, 80 % (250 ms exposure) GFP and 80 % (1 s) RFP at 10 × magnification. VDBP-GFP fluorescence was measured in the dorsal aorta as this region has been identified as appropriate for accurately determine vascular VDBP-GFP signal in zebrafish embryo-larvae and larvae. A specific segment of the dorsal aorta located in the 9th somite was defined by an ImageJ macro and measured in ImageJ for each of the samples (Supplementary Fig. 5). Fluorescence was quantified from acquired images using ImageJ (Rasband, 2011). The background of the images was subtracted from all measurements. This involved outlining the region of interest (in this case the pronephros) in each embryo-larvae using a brightfield image for anatomical reference which was then overlaid onto the fluorescence image. Fluorescence intensity for each of the bilaterally paired tubules was measured and plotted either separately (a total of 18 zebrafish per treatment; see Fig. 2 and Fig. 3) or averaged (mean) across the pair of tubules (a total of 16 zebrafish per treatment; see Supplementary Fig. 6–11).

2.7. Assessment of oxidative stress

Oxidative stress assessments were carried out on the standard 40 nm and 80 nm AuNPs in duplicate independent experiments at concentrations between 0.25 and 2 mg/L together with untreated controls (n = 12). This was repeated for modified 80 nm AuNPs at concentrations between 1 and 2 mg/L (n = 12) and between 0.25 and 0.5 mg/L (n = 6). For this, *3EpRE:hsp70:mCherry* embryo-larvae were exposed to AuNPs for 24 h from 3 dpf before imaging on a Zeiss Axio Observer Z1 at 4 dpf (see below). After exposure, animals were anaesthetised and

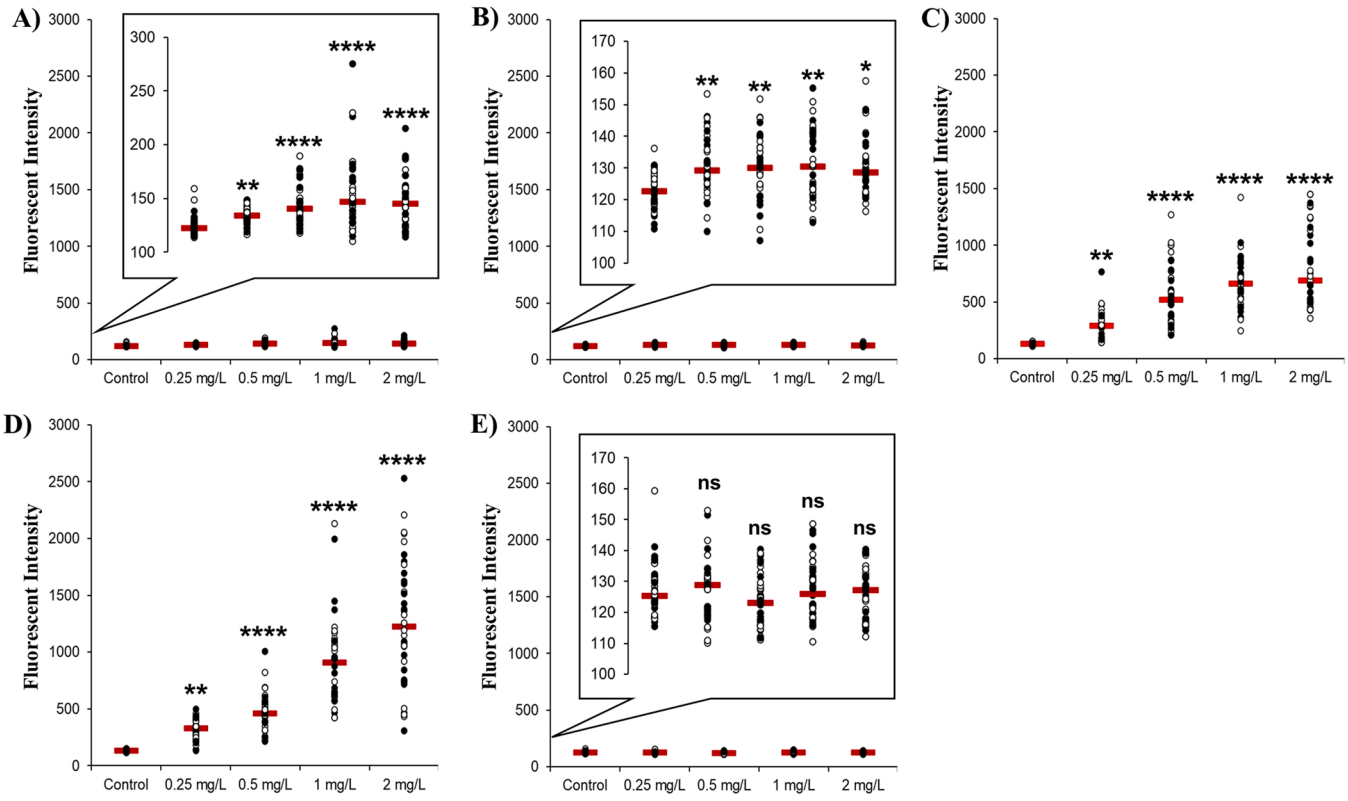

Fig. 2. Uptake of different sized AuNPs into the pronephros of zebrafish measured by fluorescence detection with SPIM. Uptake was measured in both sides of the zebrafish pronephros (white markers – right side, black markers – left side). Fish were imaged using SPIM at 4 dpf after 72 h exposure to AuNPs of sizes (a) 10 nm, (b) 20 nm, (c) 40 nm, (d) 80 nm, and (e) 100 nm. Raw data are represented as a scatter plot with means shown (indicated by the red line) for three independent experiments n = 18. (****P < 0.0001, **P < 0.01, *P < 0.05 and ns = not significant). Magnified versions of the graph are provided as figure insets for the 10 nm, 20 nm and 100 nm AuNPs to best visualise the comparatively low levels of particle uptake/fluorescence for these exposures.

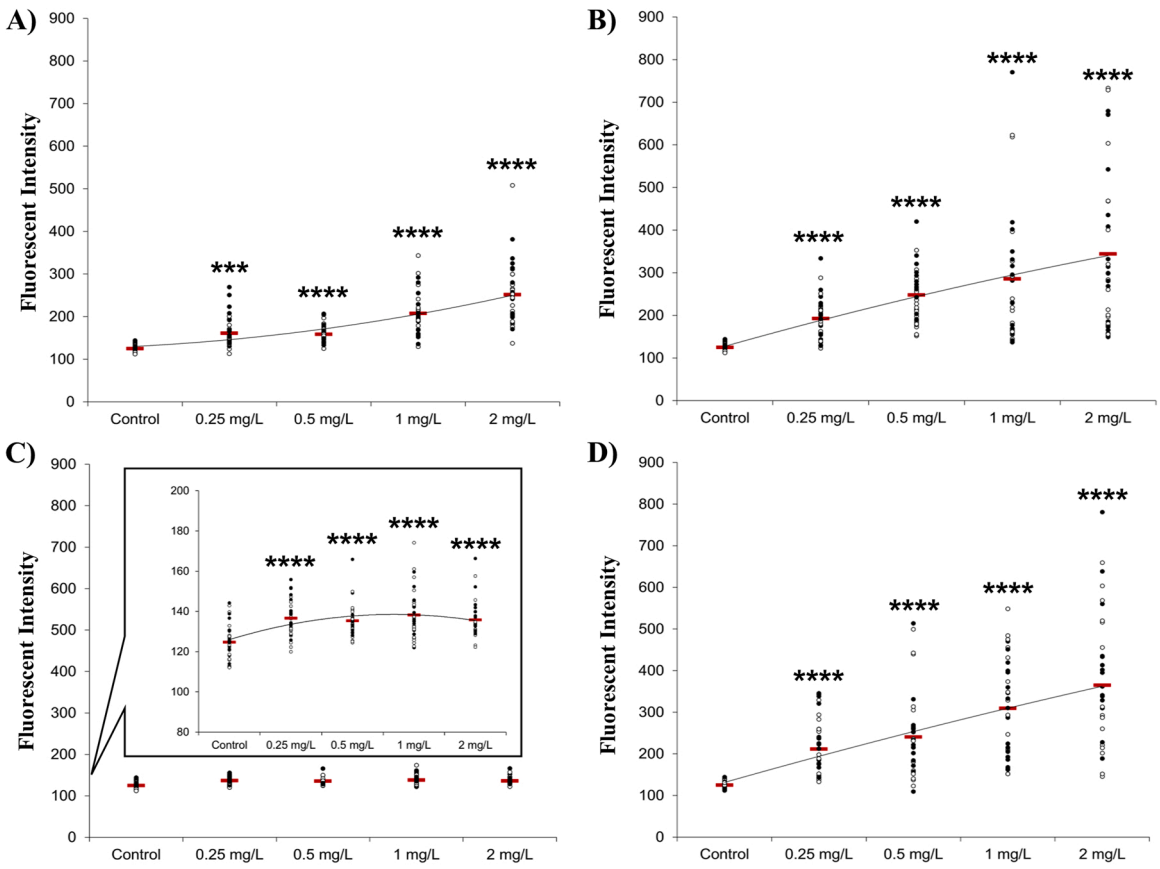

Fig. 3. Uptake of 80 nm AuNPs with different modifications as measured in the pronephros of zebrafish embryo-larvae measured via fluorescence detection with SPIM. Uptake was measured in both sides of the zebrafish pronephros (white markers – right side, black markers – left side): Fish were imaged using SPIM at 4 dpf after 72 h exposure to AuNPs. (A) Unmodified 80 nm AuNPs (B) TNF modified 80 nm AuNP (C) NHS modified 80 nm AuNP (D) PEG modified 80 nm AuNP. Raw data are represented as a scatter plot with means (shown by the red line) for three independent experiments (Kruskal-Wallis test followed by a Dunn's post hoc test; ****$P < 0.0001$). A magnified version of the graph is provided for the NHS modified AuNP to help best visualise the comparatively low levels of particle uptake/fluorescence for this exposure.

embedded as described for the renal injury assessments, and then analysed using a Zeiss Axio Observer Z1 inverted widefield fluorescence microscope equipped with an AxioCamMR3 camera and 10 ×/0.3 M27 objective. For this, Z-stacks (1388 × 1040 pixels) with 1–2 μm step size were taken through the zebrafish, imaging both brightfield and RFP with the following settings: 500 ms RFP and 1 s brightfield with a 1 × optovar. Image analysis was undertaken as detailed for the renal injury assessment above. For this work, two independent experiments were conducted, with 6 zebrafish for each AuNP concentration (0.25–2 mg/L) alongside untreated controls (n = 12).

2.8. Statistical analyses

All quantitative fluorescence intensity data were statistically analysed using a non-parametric Kruskal-Wallis test with a Dunn's post hoc test in which exposed animals in each treatment were compared with the control and between different concentrations. All statistical analyses were undertaken using GraphPad Prism 6.0 (GraphPad Software, CA, USA). Data derived from the depuration study were analysed using a Friedman test, followed by a Dunnett's post hoc test. Gold NP TEM and Zetasizer results were show as ± SD and all other data are presented as either whisker plots or as mean ± SEM. Statistically significant differences are at the $p < 0.05$ level.

3. Results

3.1. Characteristics of AuNPs

TEM analysis of the raw AuNPs (post vortex and sonication in 1 × E3 medium – to mimic the embryo-larval exposure conditions) indicated the different sized particles were uniformly spherical in shape (see Supplementary Fig. 1). TEM analysis indicated the second batch of 80 nm AuNPs were uniformly spherical in shape with a mean particle diameter in line with the sizes specified for each category by the manufacturer (see Supplementary Fig. 2). The average characteristics of 50 randomly selected AuNPs from each group are summarised in Table 1.

The size distribution analysis of the AuNPs with the Zetasizer (see Table 2 and Supplementary Fig. 13–14 for details) indicated high levels of aggregation for the 10 and 20 nm sized particles. The 40, 80, and 100 nm particles were more consistent in size within the different categories, with the larger sized particles in the different categories being consistent with the TEM measurements. The negative zeta potential (mV) readings indicate the presence of stable AuNPs whilst the higher (more neutral) readings indicate highly unstable nanoparticles, prone to aggregation. The 80 nm AuNPs were most stable followed by the 10 nm, 100 nm, 20 nm and 40 nm sized particles. For the surface modified 80 nm AuNPs, the TNF AuNPs were most stable followed by PEG AuNPs and NHS AuNPs.

Table 1
AuNP TEM analysis – primary particle diameters based on the measurement of 50 particles for each particle size/formulation.

	10 nm	20 nm	40 nm	80 nm	80 nm (Standard)	80 nm (TNFα)	80 nm (NHS)	80 nm (PEG)	100 nm
Average	14.9	20.6	41.2	76.3	76.8	75.7	79.9	74.2	105.8
Min	9.30	13.7	33.4	67.6	70.6	66.4	70.9	65.2	88.1
Max	18.7	26.3	49.8	87.7	84.7	83.7	91.1	82.1	141.2
STDEV	2.03	2.45	3.30	4.95	3.36	4.18	4.74	3.31	9.30

Table 2
Polydispersity index and zeta potential of the different sized and coated AuNPs analysed with Malvern Zetasizer (± SD).

Gold NP size (nm)	Mean diameter (STDEV/nm)	Polydispersity index (PDI) (STDEV/size)	Zeta potential (mV)
10	116.1 ± 61.8	0.65 ± 0.13	-11.9 ± 1.4
20	158.7 ± 67.7	0.71 ± 0.12	-4.67 ± 0.7
40	59.6 ± 4.2	0.22 ± 0.05	-4.05 ± 1.1
80	103.8 ± 6.0	0.13 ± 0.06	-13.3 ± 1.7
80 (Standard)	97.9 ± 4.3	0.11 ± 0.05	-14.3 ± 0.6
80 (PEG)	81.1 ± 3.6	0.19 ± 0.04	-8.15 ± 0.3
80 (TNF)	91.6 ± 4.4	0.17 ± 0.02	-12.3 ± 0.4
80 (NHS)	83.3 ± 13.0	0.53 ± 0.15	-6.69 ± 1.5
100	74.3 ± 2.3	0.41 ± 0.11	-8.83 ± 0.6

3.2. Effect of particle size on AuNP uptake and tissue partitioning

Across particle sizes 10–80 nm, we observed uptake and accumulation of AuNPs predominately in the pronephric tubules and the gut. No uptake was observed in any animals exposed to the 100 nm AuNPs. Fluorescence was also observed in the heart in some individuals exposed to 80 nm at the highest particle exposure concentration (Fig. 4). Although AuNPs uptake may have occurred in other tissues at levels below the SPIM detection limit, we were also not able to observe any particles of this size using high sensitivity/resolution confocal microscopy (see Fig. 5). There were differences in the levels of accumulation of the different sized (10–80 nm) AuNPs, but for any given exposure there was no difference detected between the levels of accumulation across left and right pronephric tubules (Fig. 4). For all particle sizes, fluorescence levels detected in the pronephros were higher than in controls at all exposure concentrations and were highest in the high concentration of 80 nm AuNPs. In the case of the 10 nm and 20 nm AuNPs, there was no clear concentration-dependent response in the tubules with a low level of fluorescence recorded across all concentrations. Illustrating this, fluorescence in the pronephric tubules in animals exposed to 40 nm and 80 nm AuNP was generally between 4 and 5 times higher than for the smaller sized AuNPs.

Accumulation of 40 and 80 nm AuNPs in the pronephric tubules was confirmed by confocal microscopy and shown to be especially prominent in the anterior part of the proximal convoluted tubule (see Fig. 4 and Fig. 5).

3.3. Effect of surface modification on AuNP uptake and tissue distribution

The uptake of modified compared to unmodified (Control) 80 nm AuNPs is shown in Fig. 3. Again, in all cases AuNP accumulation was seen only in the pronephros and gut. For the NHS modified AuNP, uptake was low compared with the standard particles (see Fig. 3C) with no clear concentration-dependent accumulation. For the highest exposure concentration of NHS modified AuNPs, the level of kidney tubule fluorescence was approximately half that for the standard 80 nm AuNPs. Conversely, for the AuNPs modified with PEG and TNF there were higher levels of accumulation in the pronephros compared with the standard AuNPs across the full tested concentration range. Illustrating this, for the highest exposure concentration (2 mg/L) uptake was 31 % higher in the PEG coated AuNPs (365 ± 28; $p < 0.0001$) and 27 % higher for the TNF modified AuNPs (344 ± 30.6; $p < 0.0001$) compared with the unmodified AuNPs (251 ± 11.7). Although levels of particle uptake varied between the left and right nephrons within individual fish, again no tubule was found to predominate overall.

3.4. The effect of depuration on AuNP persistence

After exposure to the 80 nm AuNPs and their subsequent transfer to clear medium, there was progressive clearance of particles from the pronephros over time (Fig. 6 and Supplementary Fig. 7). For example, in the 1 mg/L and 2 mg/L treatment groups, levels of fluorescence were reduced by 25 % and 16 %, respectively 24 h after removal from the exposures. After 96 h in clean water, fluorescent levels in the pronephros in the 0.25 mg/L, 0.5 mg/L, 1 mg/L and 2 mg/L treatment groups were reduced by 28 %, 46 %, 54 % and 68 %, respectively. Similar clearance rates were recorded with the 40 nm AuNPs with 44 % and 43 % reduction in pronephric fluorescence in the 1 mg/L and 2 mg/L treatments, respectively (see Supplementary Figs. 6 D&E).

For animals exposed to the TNF modified AuNPs, fluorescence was reduced by 9 %, 6.5 %, 27 % and 34 % for the 0.25, 0.5, 1 and 2 mg/L exposures respectively (see Fig. 6A and Supplementary Fig. 11). Similar levels of clearance were recorded after 96 h in clean water also for PEG modified 80 nm AuNPs levels of clearance after 96 h were 10 %, 21 %, 29 % and 36 % for the 0.25, 0.5, 1 and 2 mg/L exposures respectively (Fig. 6B and Supplementary Fig. 10). The low level of uptake/accumulation of the unmodified and NHS modified 80 nm AuNPs in this study precluded any effective elimination rate analyses.

3.5. Effects of AuNP exposure on the pronephros and on cellular oxidative stress levels

There was no significant change in the VDBP-GFP fluorescence measured in the dorsal aorta in embryo-larvae treated with 40 and 80 nm AuNPs compared with the control group, suggesting the absence of an adverse effect on GFB integrity (see Supplementary Fig. 5A&B). A further study performed with 10, 20 and 100 nm particles also indicated no effect on GFB for these sizes of AuNP also (see Supplementary Fig. 5C). There were also no significant changes in the VDBP-GFP fluorescence in the dorsal aorta in animals exposed to all standard and modified AuNPs (see Supplementary Fig. 5D–G) and no observed alterations in tubulars structure or podocyte RFP fluorescence in any of the animals assessed.

Assessment of EpRE-related mCherry fluorescence levels in animals exposed to 40 nm and 80 nm AuNPs for 24 h also revealed no evidence of induced cellular oxidative stress (Fig. 7). Similarly, no detectible changes in mCherry fluorescence were detected after exposure to the surface modified 80 nm AuNPs (see Supplementary Fig. 5D–G).

4. Discussion

Here we show that particle size and surface coating affect the bioavailability and clearance of AuNPs in zebrafish (*Danio rerio*) following aqueous exposure. Our data suggest that 40 nm and 80 nm AuNPs were taken up most readily into tissues, in a concentration-dependent manner, and that these particles predominantly accumulated in the proximal convoluted tubule of the pronephric kidney. Accumulation of AuNPs of this size range also occurred in the gut, and to a far lesser extent (in a few animals only) in the heart (within the

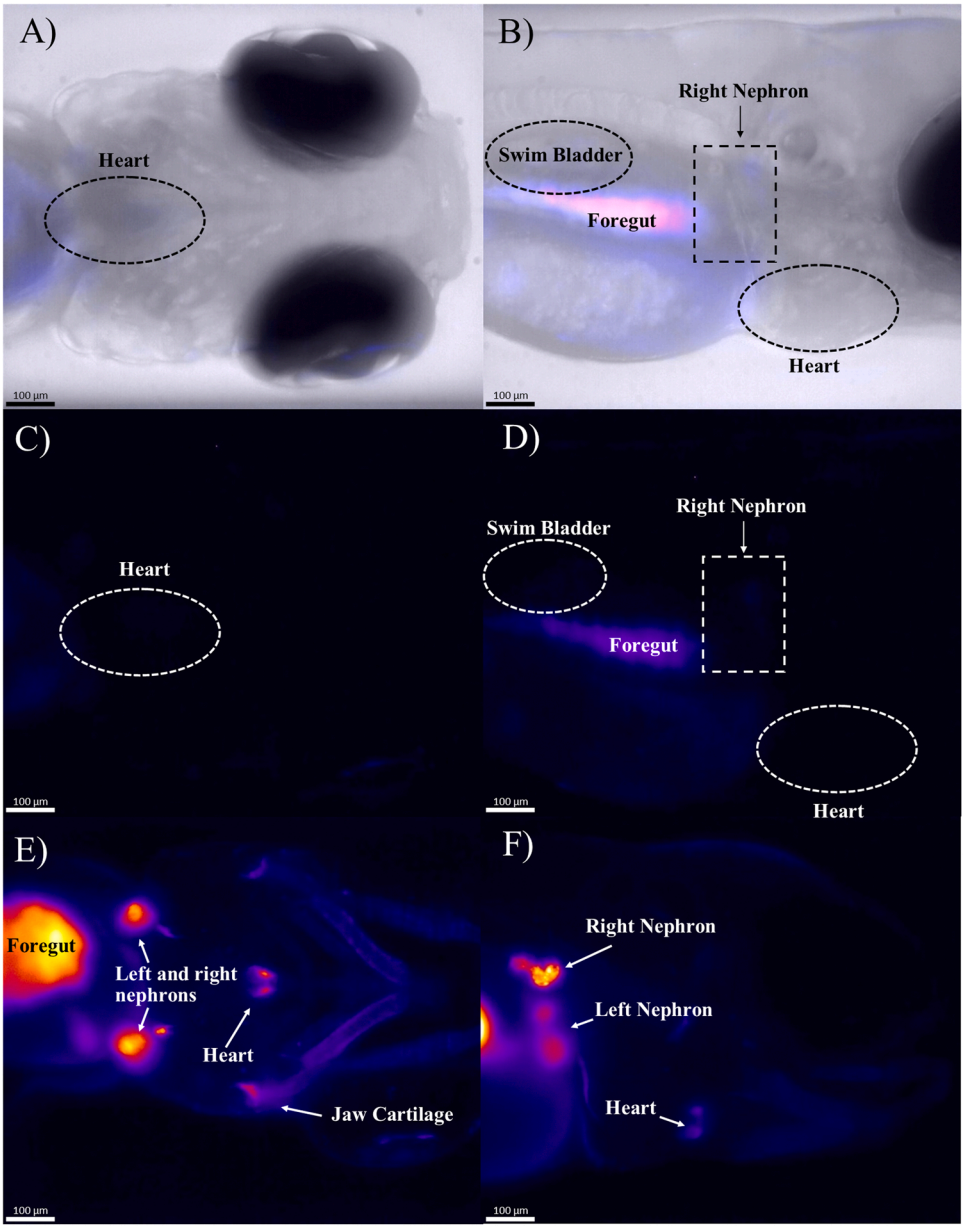

Fig. 4. SPIM images of *Casper* zebrafish embryo-larvae at 20 ×. Non-exposed controls (A–D) and zebrafish embryo-larvae exposed to 2 mg/L 80 nm AuNPs (E–F). Brightfield imaging of the control provided a reference for specific organs with autofluorescence overlaid (A–B). The non-exposed, control embryo-larvae showed minimal fluorescence in both ventral and dorsal view (C & D respectively). The exposed embryo-larvae showed AuNP accumulation in the heart and the jaw cartilage (E). In the profile view (F), fluorescence can be seen in the jaw, in the right nephron and (blurred image) in the left nephron. Autofluorescence is visible in the gut (D) but the fluorescent signal is significantly higher in the AuNP exposed zebrafish (E & F).

ventricle myocardium) and jaw cartilage at high exposure concentrations.

In our study, all sizes showed evidence of uptake and accumulation except for the 100 nm AuNPs, where a lack of visible particle fluorescence suggested poor absorption across body surfaces. Although some previous studies have investigated the influence of particle size on AuNP uptake in fish, wide variations in the coatings, experimental approaches, endpoints, and animal ages used makes comparisons between these studies and our own here extremely difficult. In one study (Browning et al., 2013), for example, aqueous exposure of zebrafish (< 2 dpf to 120 hpf) to 86.2 ± 10.8 nm AuNPs across a concentration range of 0–78 mg/L, resulted in accumulation in the retina, gills, and the tail musculature, with various deformities reported at the highest concentrations. The same researchers also exposed zebrafish of this age to smaller AuNPs (11.6 ± 0.9 nm), at concentrations ranging from 0 to 12.6 mg/L, and found that these accumulated in retina, brain, olfactory epithelium and the swim bladder (Browning et al., 2009). The number of particles taken up into those tissues, however, was low (less than 100 visible in any tissue), even at an exposure concentration of 12.6 mg/L, which is more than 6 times higher than the highest exposure regime adopted in the present study. The AuNPs used in the studies of Browning et al. (2009) were also synthesised from chloroauric acid and sodium citrate which produced non-spherical nanoparticles and thus their shape differed considerably to the spherical particles used in our study. Any one of these factors could have contributed to the different tissue distribution of NPs in our study versus this previous work. One thing that is clear from our work, however, is that although uptake and accumulation of AuNPs occurs across a wide range of nanoparticles sizes, the smaller AuNPs (10 and 20 nm particles) appear to accumulate less readily, perhaps due to more rapid elimination compared with the larger sized 40 nm and 80 nm AuNPs. Furthermore, the lack of uptake of 100 nm AuNPs in exposed zebrafish also suggests that these larger sized nanoparticles are not effectively absorbed by embryonic zebrafish. This was further supported by a lack of signal from the gut lumen of animals exposed to the 100 nm particles suggesting a relative lack of ingestion, and/or potentially a rapid exclusion from the gut. At present it is not clear what the dominant route(s) of uptake of AuNPs into zebrafish are from the water, which may include via the skin, gills, and/or orally. It is

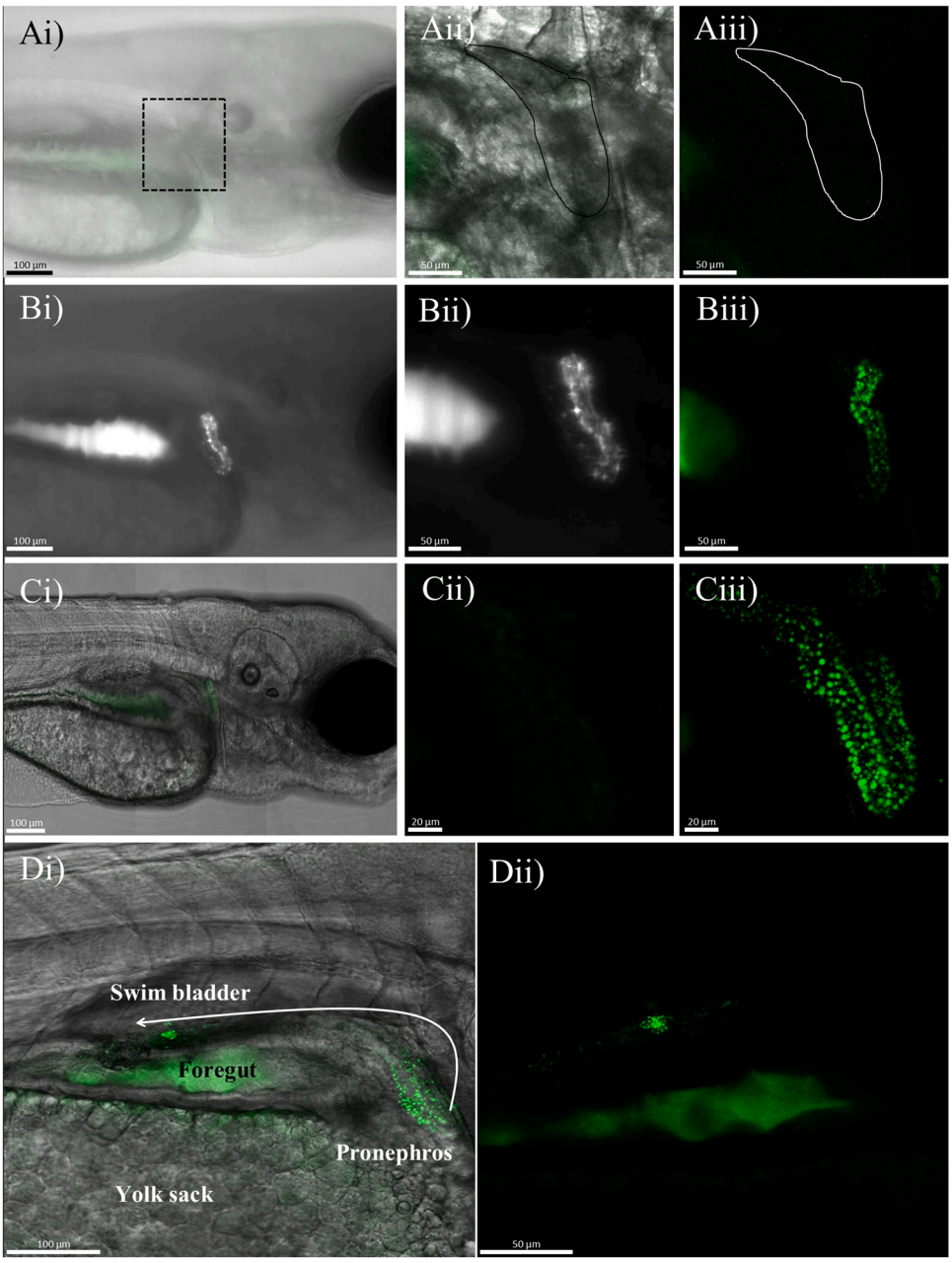

Fig. 5. Confocal imaging of AuNP fluorescence in 4 dpf zebrafish embryo-larvae. (A) Max intensity z-stacks of a *Casper* embryo-larvae control using both SPIM (Ai) and confocal microscopy (Aii/Aiii) both indicating low levels of autofluorescence. The drawn white outline indicates the position of the pronephros. (B) Max intensity z-stacks of a *Casper* embryo-larvae exposed to 2 mg/L of 80 nm AuNPs for 72 hrs using SPIM with (Bi) and without brightfield (Bii) and confocal microscopy (Biii) indicating little difference in signal sensitivity between the two microscopic techniques. (C) AiryScan max intensity z-stacks of 4 dpf *Casper* embryo-larvae after exposure to 72 hr to PEG coated 80 nm AuNPs. (Ci) A stitched max intensity image of the embryo-larvae indicating fluorescence in the pronephros. (Cii) Pronephros in *Casper* control embryo-larvae showing background fluorescence. (Ciii) Uptake of PEG coated 80 nm AuNPs visualised in the pronephros. (D) A max intensity confocal Z stack of a *Casper* zebrafish embryo-larvae exposed to 2 mg/L 80 nm AuNPs for 72 h showing their presence in the pronephros (Di, 10 ×) and in the proximal straight tubule/proximal early segment of the pronephros (Dii, 20 ×).

highly likely that the primary route of uptake is dependent also on the age of animals. For example, in larval fish in which the surface area to volume ratio is large, and where skin is relatively permeable, the body surface is likely to represent a more dominant route compared with the gills. Conversely, in adult fish, changes in skin permeability and development of mature ion transport systems may lead to an increase in the relative importance of the gills in the absorption of (in particular) charged or biocompatible NPs (Handy et al., 2008). Similarly, ingestion is likely to become more important in actively feeding animals compared with pre 4 dpf zebrafish. In support of this, in a study undertaken with 4 week old zebrafish, animals exposed to fluorescently labelled 89 ± 21 nm AuNPs (1 mg/L for 3 days) showed fluorescence only in the gut (Skjolding et al., 2017). These data further illustrate the importance of clear reporting on methodological and particle details for uptake studies with nanoparticles to allow for appropriate comparisons.

We found surface modifications of the 80 nm sized AuNPs with both PEG and TNF enhanced their uptake and retention into the kidney pronephros compared with unmodified AuNPs of the same size. These modifications, however, did not affect tissue distribution patterns in the exposed zebrafish embryo-larvae, as the pronephros and gut were the predominant sites of accumulation similarly to noncoated AuNPs. The enhanced uptake of PEG coated AuNPs is particularly concerning due to the extensive use of PEG for enhancing biocompatibility in AuNPs and the FDA approval of PEG in protein drugs (Alconcel et al., 2011; Karakoti et al., 2011). Smaller sized PEG coated AuNPs (8–15 nm) have been shown to have higher toxicity compared to polymer coating in zebrafish embryo-larvae (exposed from 3 to 96 hpf) at relatively low doses (< 1 nM (Floris et al., 2021).

To our knowledge, no studies have shown an effect of TNF-coating on AuNP bioavailability in aquatic organisms. Studies investigating the effect of TNFα conjugated CYT-6091, (27 nm TNFα/PEG AuNP) in rabbit kidney tumour (Pedro et al., 2010) and murine models (Goel et al., 2009) have, however, previously shown an enhanced accumulation in tumour tissues. In contrast with PEG and TNF, we showed surface modifications with NHS (with PAMAM attachments) resulted in a lower level of uptake in the pronephros compared to that of the unmodified

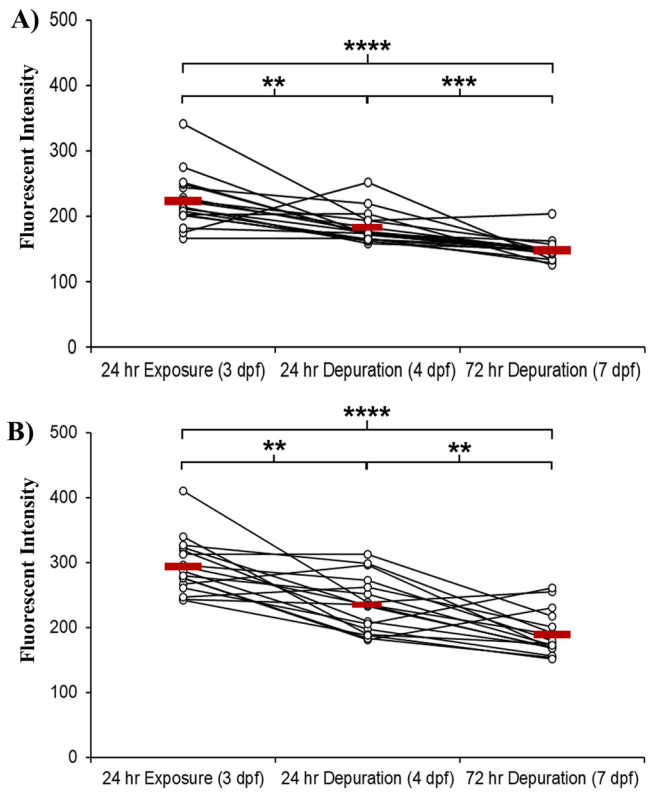

Fig. 6. Clearance of 80 nm AuNPs (exposed at 2 mg/L) from the pronephros of zebrafish embryo-larvae measured by fluorescence detection with SPIM with the data presented as scatter plots. Fluorescence was measured in both sides of the zebrafish embryo-larvae pronephros and averaged for each individual fish. The same fish were recorded over the 72 hr depuration period. Fluorescence was measured at 3 dpf, after the 24 h exposure, and subsequently at two depuration time points (after a further 24 hr and 72 h): (A) TNF modified AuNP (B) PEG modified AuNP. Raw data are represented as individual fish with means shown (as red lines) for two independent experiments n = 12. (Friedman test, followed by a Dunnett's post hoc test; ****$P < 0.0001$, ***$P < 0.001$ and **$P < 0.01$).

AuNPs. The PAMAM dendrimers were conjugated with the NHS AuNPs, which consists of an alkyl-diamine core with tertiary amine branches and 4 surface groups. As the G0 PAMAM dendrimers measure only 1.5 nm in hydrodynamic diameter, we speculate that potential changes in the planar and elliptical shape may have affected their uptake into the zebrafish embryo-larvae (Bahadır and Sezgintürk, 2016). Our data add to other findings showing that surface modifications can play a major role in bioavailability and tissue distribution of AuNPs in zebrafish (Harper et al., 2011, 2014; Truong et al., 2012, 2019; Kim et al., 2013; Ginzburg et al., 2018; Sung et al., 2018; Van Pomeren et al., 2019).

Clearance of standard 40 and 80 nm AuNPs occurred at similar rates for the exposure concentrations where this was most easily measured (1 mg/L and 2 mg/L). These data suggest that both 40 and 80 nm AuNPs were excreted, though some of these particles (as measured by fluorescence) persisted in the pronephros even 4 days after transfer of the embryo-larvae to fresh water. This was also the case for the 80 nm AuNPs with PEG and TFNα surface modifications (Fig. 6). AuNP persistence raises questions as to the potential for chronic effects of tissue accumulation, particularly with regards to the kidney. Similar persistence has been shown in mice studies exposed to 60 and 100 nm PEG-coated AuNPs (Cho et al., 2009; Zhang et al., 2011). Clearance of AuNPs in fish have been reported elsewhere for AuNPs of different sizes and surface modifications. For example, elimination from the Japanese medaka gut was shown to occur within 24 h after aqueous exposure to 2 nm AuNP with various hydrophilic conjugations (measuring 6–14 nm), with a slower clearance rate for cationic NPs (Zhu et al., 2010). Similarly, in a study with 2–3 month old zebrafish injected intraperitoneally with 17–21 nm AuNPs (at 5 μg/g), particles were taken up into the digestive system, swim bladder and the heart (low levels). The majority of these particles were found to be excreted within 48 h (Sangabathuni et al., 2017). In the latter study, PEG-coated AuNPs cleared at a faster rate compared to those coated with mannose. Interestingly, studies on dietary AuNP exposure in zebrafish have indicated different excretion routes for different sized AuNPs. For example, Geffroy et al. reported that 50 nm particles were excreted in the faeces whereas smaller particles (12 nm AuNP) were not and were likely cleared via urinary excretion (Geffroy et al., 2012). This may help explain some of our findings on embryo-larval stages of zebrafish where the smaller AuNPs (10–20 nm) were not found to accumulate in the pronephros, whereas the larger sized (40 nm and 80 nm) particles did. Overall, our data agree with previous studies that AuNPs of various sizes and coatings are relatively rapidly cleared from zebrafish following their uptake, however we show too that certain coating types may increase their persistence, warranting further systematic investigation to more fully understand this.

Despite the apparent accumulation of 40 and 80 nm AuNPs over 72 h, we found no detectable effect on pronephros structure/function, cellular oxidative stress, or morphology. Nanoparticle data in the literature are widely conflicting with regards to AuNPs toxicity. For example, in contrast with our findings, exposure to a relatively low concentration of 46 nm AuNPs (0.11 nM), versus our max dosing of 0.34 nM, has been reported to cause mortality in 56 and 80 hpf zebrafish embryo-larvae (Wang et al., 2016). In zebrafish embryo-larvae exposed to 75–97 nm AuNP at concentrations up to 78 μg/ml (for 120 h), low levels of mortality and embryonic deformity were reported by Browning et al. (2013). Conversely, Bar-Ilan et al. (2009) found no toxicity in zebrafish embryo-larvae exposed for 5 dpf to 250 μM of 3, 10, 50 and 100 nm AuNPs. Difference in the nature of the AuNPs used may explain the distinct results of these studies: Bar-Ilan et al. (2009) included the addition of a ligand stabiliser (TPPMS) whereas Wang et al. (2016) used cetyltrimethylammonium bromide as a stabiliser.

In rats, bioaccumulation of AuNPs (5–50 nm) after repeated dosing has not been found to cause measurable levels of nephrotoxicity (Abdelhalim and Moussa, 2013; Jo et al., 2015; Rambanapasi et al., 2016). In contrast, AuNP dietary exposures in adult zebrafish to 12 nm AuNPs (36 days at 90 ng AuNPs per fish per day) have been shown to induce ROS (as measured through induction of the *sod2* gene) in muscles (Geffroy et al. (2012). Furthermore, exposure via the sediment to 14 nm citrate-capped AuNPs at 0.8 μg/L over 20 days resulted in *sod2* induction in the brain (Dedeh et al., 2015). However, this study showed a down-regulation of *sod2* in the muscle (0.8 μg/L) and gill (0.25 and 0.8 μg/L). Here, we observed no indication that our tested particles caused cellular oxidative stress or affected pronephric organ function. This may be due to the non-reactive methyl polymer layer coating on the AuNPs which most likely reduced or eliminated any potential particle disassociation (Au ions) thus preventing ROS production.

In both the UK and USA, consumption of medical AuNPs are estimated at 540 kg and 2700 kg, respectively, based on analyses of AuNP clinical applications, sewage treatment plants and hazardous waste compartment (landfills). Further, the highest concentration of AuNP in surface water and sewage plant effluents is estimated at 670 pg/L (Mahapatra et al., 2015). Thus, AuNP concentrations inducing toxic effects for any reported study in zebrafish to date are beyond immediate environmentally relevance.

In conclusion, we show a size-selective uptake of AuNPs in zebrafish embryo-larvae exposed aqueously, and a preferential accumulation of particles in the pronephric tubules and gastrointestinal tract. In the case of the pronephric tubules, particle uptake persisted suggesting the potential for long term accumulation under conditions of chronic exposure. We also show that surface modifications of the AuNP with PEG and TNFα alters AuNP bioavailability in zebrafish embryo-larvae

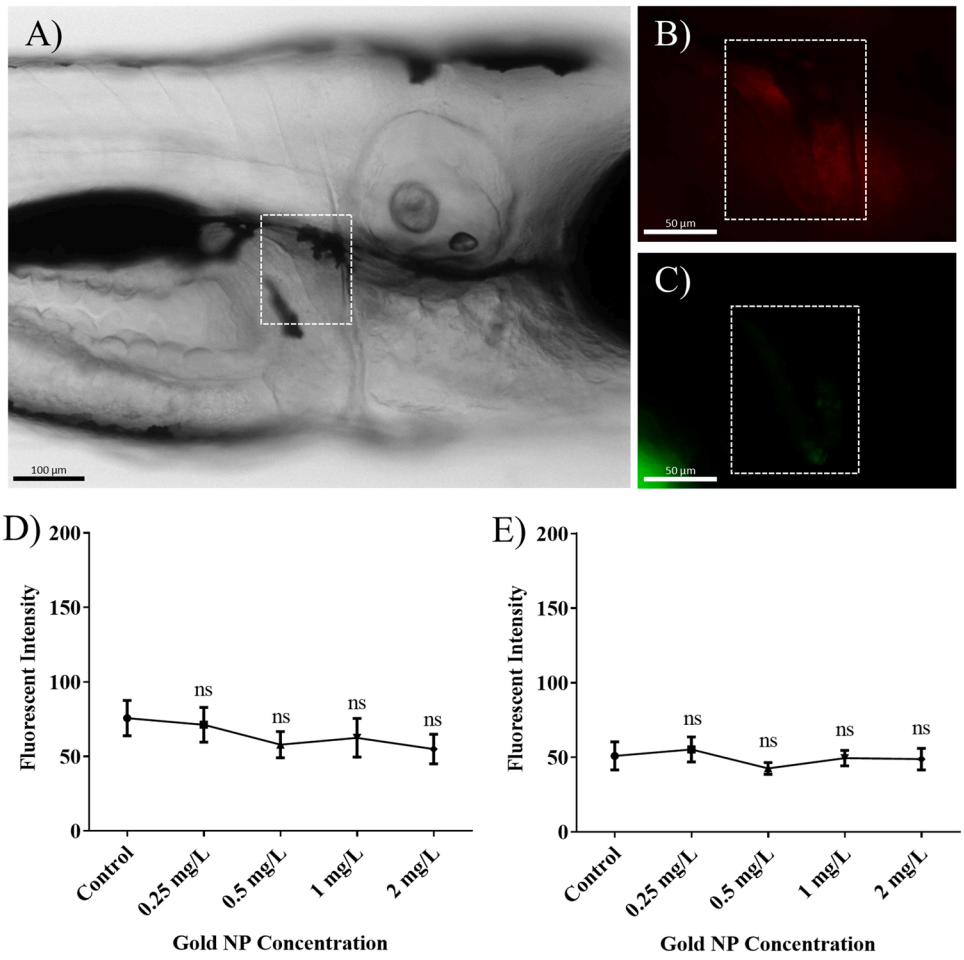

Fig. 7. Oxidative stress indicated by mCherry fluorescence measured in 3*EpRE*:hsp70:mCherry zebrafish embryo-larvae after exposure to AuNPs for 24 h. The kidney outline is highlighted over the brightfield image (A) and over the red fluorescence (mCherry) detection image (B). The fluorescence signal from the AuNPs is faintly visible in (C). These Zeiss Inverted images are for *EpRE* zebrafish embryo-larvae exposed to 2 mg/L 80 nm AuNPs. Data for exposure to (D) 40 nm and (E) 80 nm AuNPs are represented as means ± SEM for two independent experiments n = 12. (Kruskal-Wallis test followed by a Dunn's post hoc test; ns = not significant).

emphasising the importance of coatings in considerations for potential ecotoxicological effects. Despite this clear evidence for uptake and accumulation, however, we found no evidence of toxicity regardless of AuNP size or surface modifications. Collectively, these data suggest a low potential impact on fish in natural environments, particularly given that environmental concentrations are generally far below those used here and in previous studies in which toxic effects have been recorded. Nevertheless, our exposure studies were relatively short term and given the potential for accumulation of AuNPs in fish, and the fact that their use is likely to increase with the advent of more advanced methods of drug delivery, more research into the longer-term effects of these novel environmental contaminants is warranted for providing confidence to ensure low future environmental risk.

CRediT authorship contribution statement

CRT, DW and SO conceived the project and developed the concept. CRT, JM and SO obtained the funding. DW, CRT, JM, SM and MJW designed the experiments that were all undertaken by DW who also analysed the resultant data. Data interpretation was undertaken by DW, SM, MJW, and CRT. DW, MJW and CRT wrote the manuscript, with further input from all other authors.

Funding

This work was funded by a BBSRC CASE studentship with AstraZeneca (DW, Reference no. 640055046) and funding from the University of Exeter to CRT.

Declaration of Competing Interest

SFO is an employee and shareholder of AstraZeneca PLC. All other authors declare no potentially competing interests.

Data Availability

Data will be made available on request.

Acknowledgements

This work was funded by a BBSRC CASE studentship with AstraZeneca (DW, Reference no. 640055046) and funding from the University of Exeter to CRT. The authors would like to thank the staff in the Aquatic Resources Centre at the University of Exeter, for the supply and maintenance of the zebrafish, Ana Correia da Silva in the Bioimaging Unit at the University of Exeter for conducting TEM analysis and Dr Weibin Zhou (University of Michigan, Ann Arbor) for kindly providing the *pod*::NTR-mCherry/*l-fabp*::VDBP-GFP transgenic fluorescent reporter line. David Hier Render Studio (see: http://www.davidhier.co.uk/) generated the rendered images contained within Fig. 1 of the main text, and Supplementary Fig. 3 in the Supplementary materials and Methods.

Animal Ethics statement

All work was undertaken under project and personnel licences granted by the UK Home Office under the UK Animals (Scientific Procedures) Act and approved by the University of Exeter's Animal Welfare and Ethical Review Body.

Appendix A. Supporting information

Supplementary data associated with this article can be found in the online version at doi:10.1016/j.ecoenv.2023.115019.

References

Abdelhalim, M.A.K., Moussa, S.A.A., 2013. The gold nanoparticle size and exposure duration effect on the liver and kidney function of rats: in vivo. Saudi J. Biol. Sci. 20, 177–181.

Alconcel, S.N., Baas, A.S., Maynard, H.D., 2011. FDA-approved poly (ethylene glycol)–protein conjugate drugs. Polym. Chem. 2, 1442–1448.

Aryal, S., Grailer, J.J., Pilla, S., Steeber, D.A., Gong, S., 2009. Doxorubicin conjugated gold nanoparticles as water-soluble and pH-responsive anticancer drug nanocarriers. J. Mater. Chem. 19, 7879–7884.

Bahadır, E.B., Sezgintürk, M.K., 2016. Poly (amidoamine)(PAMAM): an emerging material for electrochemical bio (sensing) applications. Talanta 148, 427–438.

Bar-Ilan, O., Albrecht, R.M., Fako, V.E., Furgeson, D.Y., 2009. Toxicity assessments of multisized gold and silver nanoparticles in zebrafish embryos. Small 5, 1897–1910.

Botha, T.L., James, T.E., Wepener, V., 2015. Comparative aquatic toxicity of gold nanoparticles and ionic gold using a species sensitivity distribution approach. J. Nanomater. 2015, 11.

Boyles, M.S., Kristl, T., Andosch, A., Zimmermann, M., Tran, N., Casals, E., Himly, M., Puntes, V., Huber, C.G., Lütz-Meindl, U., 2015. Chitosan functionalisation of gold nanoparticles encourages particle uptake and induces cytotoxicity and pro-inflammatory conditions in phagocytic cells, as well as enhancing particle interactions with serum components. J. Nanobiotechnol. 13, 84.

Bozich, J.S., Lohse, S.E., Torelli, M.D., Murphy, C.J., Hamers, R.J., Klaper, R.D., 2014. Surface chemistry, charge and ligand type impact the toxicity of gold nanoparticles to Daphnia magna. Environ. Sci.: Nano 1, 260–270.

Browning, L.M., Lee, K.J., Huang, T., Nallathamby, P.D., Lowman, J.E., Xu, X.-H.N., 2009. Random walk of single gold nanoparticles in zebrafish embryos leading to stochastic toxic effects on embryonic developments. Nanoscale 1, 138–152.

Browning, L.M., Huang, T., Xu, X.-H.N., 2013. Real-time in vivo imaging of size-dependent transport and toxicity of gold nanoparticles in zebrafish embryos using single nanoparticle plasmonic spectroscopy. Interface Focus 3, 20120098.

Carnovale, C., Bryant, G., Shukla, R., Bansal, V., 2016. Size, shape and surface chemistry of nano-gold dictate its cellular interactions, uptake and toxicity. Prog. Mater. Sci. 83, 152–190.

Chen, J., Chen, X., Xu, R., Zhu, Y., Shi, Y., Zhu, X., 2008. Refractive index of aqueous solution of CdTe quantum dots. Opt. Commun. 281, 3578–3580.

Chithrani, B.D., Ghazani, A.A., Chan, W.C., 2006. Determining the size and shape dependence of gold nanoparticle uptake into mammalian cells. Nano Lett. 6, 662–668.

Cho, W.-S., Kim, S., Han, B.S., Son, W.C., Jeong, J., 2009. Comparison of gene expression profiles in mice liver following intravenous injection of 4 and 100 nm-sized PEG-coated gold nanoparticles. Toxicol. Lett. 191, 96–102.

Choi, C.H.J., Alabi, C.A., Webster, P., Davis, M.E., 2010. Mechanism of active targeting in solid tumors with transferrin-containing gold nanoparticles. Proc. Natl. Acad. Sci. 107, 1235–1240.

Corsi, I., Cherr, G.N., Lenihan, H.S., Labille, J., Hassellov, M., Canesi, L., Dondero, F., Frenzilli, G., Hristozov, D., Puntes, V., 2014. Common Strategies and Technologies for the Ecosafety Assessment and Design of Nanomaterials Entering the Marine Environment. ACS Publications.

Daraee, H., Eatemadi, A., Abbasi, E., Fekri Aval, S., Kouhi, M., Akbarzadeh, A., 2016. Application of gold nanoparticles in biomedical and drug delivery. Artif. Cells Nanomed. Biotechnol. 44, 410–422.

Dedeh, A., Ciutat, A., Treguer-Delapierre, M., Bourdineaud, J.-P., 2015. Impact of gold nanoparticles on zebrafish exposed to a spiked sediment. Nanotoxicology 9, 71–80.

Dominguez, G.A., Lohse, S.E., Torelli, M.D., Murphy, C.J., Hamers, R.J., Orr, G., Klaper, R.D., 2015. Effects of charge and surface ligand properties of nanoparticles on oxidative stress and gene expression within the gut of Daphnia magna. Aquat. Toxicol. 162, 1–9.

Floris, P., Garbujo, S., Rolla, G., Giustra, M., Salvioni, L., Catelani, T., Colombo, M., Mantecca, P., Fiandra, L., 2021. The role of polymeric coatings for a safe-by-design development of biomedical gold nanoparticles assessed in zebrafish embryo. Nanomaterials 11, 1004.

Fratoddi, I., Venditti, I., Cametti, C., Russo, M.V., 2015. How toxic are gold nanoparticles? The state-of-the-art. Nano Res. 8, 1771–1799.

García-Fernández, L., Garcia-Pardo, J., Tort, O., Prior, I., Brust, M., Casals, E., Lorenzo, J., Puntes, V.F., 2017. Conserved effects and altered trafficking of Cetuximab antibodies conjugated to gold nanoparticles with precise control of their number and orientation. Nanoscale 9, 6111–6121.

Geffroy, B., Ladhar, C., Cambier, S., Treguer-Delapierre, M., Brèthes, D., Bourdineaud, J.-P., 2012. Impact of dietary gold nanoparticles in zebrafish at very low contamination pressure: the role of size, concentration and exposure time. Nanotoxicology 6, 144–160.

Ginzburg, A.L., Truong, L., Tanguay, R.L., Hutchison, J.E., 2018. Synergistic toxicity produced by mixtures of biocompatible gold nanoparticles and widely used surfactants. ACS Nano 12, 5312–5322.

Goel, R., Shah, N., Visaria, R., Paciotti, G.F., Bischof, J.C., 2009. Biodistribution of TNF-α-coated gold nanoparticles in an in vivo model system. Nanomedicine 4, 401–410.

Handy, R.D., Henry, T.B., Scown, T.M., Johnston, B.D., Tyler, C.R., 2008. Manufactured nanoparticles: their uptake and effects on fish—a mechanistic analysis. Ecotoxicology 17, 396–409.

Harper, B., Sinche, F., Ho Wu, R., Gowrishankar, M., Marquart, G., Mackiewicz, M., Harper, S.L., 2014. The impact of surface ligands and synthesis method on the toxicity of glutathione-coated gold nanoparticles. Nanomaterials 4, 355–371.

Harper, S.L., Carriere, J.L., Miller, J.M., Hutchison, J.E., Maddux, B.L., Tanguay, R.L., 2011. Systematic evaluation of nanomaterial toxicity: utility of standardized materials and rapid assays. ACS Nano 5, 4688–4697.

Jo, M.-R., Bae, S.-H., Go, M.-R., Kim, H.-J., Hwang, Y.-G., Choi, S.-J., 2015. Toxicity and biokinetics of colloidal gold nanoparticles. Nanomaterials 5, 835–850.

Karakoti, A.S., Das, S., Thevuthasan, S., Seal, S., 2011. PEGylated inorganic nanoparticles. Angew. Chem. Int. Ed. 50, 1980–1994.

Khan, A., Rashid, R., Murtaza, G., Zahra, A., 2014. Gold nanoparticles: synthesis and applications in drug delivery. Trop. J. Pharmaceut. Res. 13, 1169–1177.

Khosravi-Katuli, K., Prato, E., Lofrano, G., Guida, M., Vale, G., Libralato, G., 2017. Effects of nanoparticles in species of aquaculture interest. Environ. Sci. Pollut. Res. 24, 17326–17346.

Kim, K.-T., Zaikova, T., Hutchison, J.E., Tanguay, R.L., 2013. Gold nanoparticles disrupt zebrafish eye development and pigmentation. Toxicol. Sci. 133, 275–288.

Lee, S.H., Bae, K.H., Kim, S.H., Lee, K.R., Park, T.G., 2008. Amine-functionalized gold nanoparticles as non-cytotoxic and efficient intracellular siRNA delivery carriers. Int. J. Pharmaceut. 364, 94–101.

Leopold, L.F., Tódor, I.S., Diaconeasa, Z., Ruginǎ, D., Ştefancu, A., Leopold, N., Coman, C., 2017. Assessment of PEG and BSA-PEG gold nanoparticles cellular interaction. Colloids Surf. A: Physicochem. Eng. Asp. 532, 70–76.

Libralato, G., Galdiero, E., Falanga, A., Carotenuto, R., De Alteriis, E., Guida, M., 2017. Toxicity effects of functionalized quantum dots, gold and polystyrene nanoparticles on target aquatic biological models: a review. Molecules 22, 1439.

Mahapatra, I., Sun, T.Y., Clark, J.R., Dobson, P.J., Hungerbuehler, K., Owen, R., Nowack, B., Lead, J., 2015. Probabilistic modelling of prospective environmental concentrations of gold nanoparticles from medical applications as a basis for risk assessment. J. Nanobiotechnol. 13, 93.

Manivasagan, P., Bharathiraja, S., Bui, N.Q., Lim, I.G., Oh, J., 2016. Paclitaxel-loaded chitosan oligosaccharide-stabilized gold nanoparticles as novel agents for drug delivery and photoacoustic imaging of cancer cells. Int. J. Pharmaceut. 511, 367–379.

Mourabit, S., Fitzgerald, J.A., Ellis, R.P., Takesono, A., Porteus, C.S., Trznadel, M., Metz, J., Winter, M.J., Kudoh, T., Tyler, C.R., 2019. New insights into organ-specific oxidative stress mechanisms using a novel biosensor zebrafish. Environ. Int. 133, 105138.

Nejdl, L., Richtera, L., Xhaxhiu, K., Kensova, R., Kudr, J., Ruttkay-Nedecky, B., Kynicky, J., Wawrzak, D., Adam, V., Kizek, R., 2016. UV tuning of cadmium telluride quantum dots (CdTe QDs)–assessed by spectroscopy and electrochemistry. Int. J. Electrochem. Sci. 11, 175–188.

Nicol, J.R., Dixon, D., Coulter, J.A., 2015. Gold nanoparticle surface functionalization: a necessary requirement in the development of novel nanotherapeutics. Nanomedicine 10, 1315–1326.

Oh, E., Delehanty, J.B., Sapsford, K.E., Susumu, K., Goswami, R., Blanco-Canosa, J.B., Dawson, P.E., Granek, J., Shoff, M., Zhang, Q., 2011. Cellular uptake and fate of PEGylated gold nanoparticles is dependent on both cell-penetration peptides and particle size. Acs Nano 5, 6434–6448.

Park, S., Woodhall, J., Ma, G., Veinot, J.G., Boxall, A., 2015. Do particle size and surface functionality affect uptake and depuration of gold nanoparticles by aquatic invertebrates? Environ. Toxicol. Chem. 34, 850–859.

Pedro, R.N., Thekke-Adiyat, T., Goel, R., Shenoi, M., Slaton, J., Schmechel, S., Bischof, J., Anderson, J.K., 2010. Use of tumor necrosis factor–alpha-coated gold nanoparticles to enhance radiofrequency ablation in a translational model of renal tumors. Urology 76, 494–498.

Qiu, H., Rieger, J., Gilbert, B., Jérôme, R., Jérôme, C., 2004. PLA-coated gold nanoparticles for the labeling of PLA biocarriers. Chem. Mater. 16, 850–856.

Rambanapasi, C., Zeevaart, J., Buntting, H., Bester, C., Kotze, D., Hayeshi, R., Grobler, A., 2016. Bioaccumulation and subchronic toxicity of 14 nm gold nanoparticles in rats. Molecules 21, 763.

Rasband, W.S., 2011. Imagej. US National Institutes of Health, Bethesda, Maryland, USA. ⟨http://imagej.nih.gov/ij/⟩.

Sangabathuni, S., Murthy, R.V., Chaudhary, P.M., Subramani, B., Toraskar, S., Kikkeri, R., 2017. Mapping the glyco-gold nanoparticles of different shapes toxicity, biodistribution and sequestration in adult zebrafish. Sci. Rep. 7, 4239.

Satriano, C., Munzone, A., Cucci, L.M., Giacomelli, C., Trincavelli, M.L., Martini, C., Rizzarelli, E., Mendola, D, L.A., 2018. Angiogenin-mimetic peptide functionalised gold nanoparticles for cancer therapy applications. Microchem. J. 136, 157–163.

Skjolding, L.M., Aśmonaitė, G., Jølck, R.I., Andresen, T.L., Selck, H., Baun, A., Sturve, J., 2017. An assessment of the importance of exposure routes to the uptake and internal localisation of fluorescent nanoparticles in zebrafish (*Danio rerio*), using light sheet microscopy. Nanotoxicology 11, 351–359.

Sung, H.K., Jo, E., Kim, E., Yoo, S.-K., Lee, J.-W., Kim, P.-J., Kim, Y., Eom, I.-C., 2018. Analysis of gold and silver nanoparticles internalized by zebrafish (Danio rerio) using single particle-inductively coupled plasma-mass spectrometry. Chemosphere 209, 815–822.

Truong, L., Zaikova, T., Richman, E.K., Hutchison, J.E., Tanguay, R.L., 2012. Media ionic strength impacts embryonic responses to engineered nanoparticle exposure. Nanotoxicology 6, 691–699.

Truong, L., Zaikova, T., Baldock, B.L., Balik-Meisner, M., To, K., Reif, D.M., Kennedy, Z. C., Hutchison, J.E., Tanguay, R.L., 2019. Systematic determination of the

relationship between nanoparticle core diameter and toxicity for a series of structurally analogous gold nanoparticles in zebrafish. Nanotoxicology 13, 879–893.
Van Pomeren, M., Peijnenburg, W., Vlieg, R., Van Noort, S., Vijver, M., 2019. The biodistribution and immuno-responses of differently shaped non-modified gold particles in zebrafish embryos. Nanotoxicology 13, 558–571.
Verma, S.K., Jha, E., Panda, P.K., Kumari, P., Pramanik, N., Kumari, S., Thirumurugan, A., 2018. Molecular investigation to RNA and protein based interaction induced in vivo biocompatibility of phytofabricated AuNP with embryonic zebrafish. Artif. Cells Nanomed. Biotechnol. 46, S671–S684.
Wang, Z., Xie, D., Liu, H., Bao, Z., Wang, Y., 2016. Toxicity assessment of precise engineered gold nanoparticles with different shapes in zebrafish embryos. RSC Adv. 6, 33009–33013.
White, R.M., Sessa, A., Burke, C., Bowman, T., Leblanc, J., Ceol, C., Bourque, C., Dovey, M., Goessling, W., Burns, C.E., 2008. Transparent adult zebrafish as a tool for in vivo transplantation analysis. Cell Stem Cell 2, 183–189.
Winter, M.J., Windell, D., Metz, J., Matthews, P., Pinion, J., Brown, J.T., Hetheridge, M. J., Ball, J.S., Owen, S.F., Redfern, W.S., 2017. 4-Dimensional functional profiling in the convulsant-treated larval zebrafish brain. Sci. Rep. 7, 6581.
Zhang, X.-D., Di Wu, X.S., Liu, P.-X., Yang, N., Zhao, B., Zhang, H., Sun, Y.-M., Zhang, L.-A., Fan, F.-Y., 2011. Size-dependent in vivo toxicity of PEG-coated gold nanoparticles. Int. J. Nanomed. 6, 2071.
Zhou, W., Hildebrandt, F., 2012. Inducible podocyte injury and proteinuria in transgenic zebrafish. J. Am. Soc. Nephrol. ASN, 2011080776.
Zhu, Z.J., Carboni, R., Quercio, M.J., Yan, B., Miranda, O.R., Anderton, D.L., Arcaro, K.F., Rotello, V.M., Vachet, R.W., 2010. Surface properties dictate uptake, distribution, excretion, and toxicity of nanoparticles in fish. Small 6, 2261–2265.